

# 3'-Deoxy-3'-[<sup>18</sup>F]-fluorothymidine ([<sup>18</sup>F]-FLT) transport in newly diagnosed glioma: correlation with nucleoside transporter expression, vascularization, and blood–brain barrier permeability

Aya Shinomiya · Keisuke Miyake · Masaki Okada · Takehiro Nakamura · Nobuyuki Kawai · Yoshio Kushida · Reiji Haba · Nobuyuki Kudomi · Masaaki Tokuda · Takashi Tamiya

Received: 30 September 2012 / Accepted: 31 January 2013 / Published online: 20 February 2013  
© The Japan Society of Brain Tumor Pathology 2013

**Abstract** 3'-Deoxy-3'-[<sup>18</sup>F]-fluorothymidine ([<sup>18</sup>F]-FLT), a marker of cellular proliferation, has been used in positron emission tomography (PET) examination of gliomas. The aim of this study was to investigate whether the uptake of [<sup>18</sup>F]-FLT in glioma correlates with messenger RNA (mRNA) levels of the equilibrative nucleoside transporter 1 (ENT1), microvascular density (assessed by CD34 immunohistochemistry), and the blood–brain barrier (BBB) breakdown. A total of 21 patients with newly diagnosed glioma were examined with [<sup>18</sup>F]-FLT PET. Tumor lesions were identified as areas of focally increased [<sup>18</sup>F]-FLT uptake, exceeding that of surrounding normal tissue. Dynamic analysis of [<sup>18</sup>F]-FLT PET revealed correlations between the phosphorylation rate constant  $k_3$  and ENT1 expression; however there was no correlation between the kinetic parameters and CD34 score. There was a good correlation between the gadolinium (Gd) enhancement score (evaluating BBB breakdown) and ENT1 expression, CD34 score, and Ki-67 index. This preliminary study

suggests that ENT1 expression might not reflect accumulation of [<sup>18</sup>F]-FLT in vivo due to BBB permeability in glioma.

**Keywords** [<sup>18</sup>F]-FLT · Nucleoside transporter · CD34 · Blood–brain barrier · Glioma

## Introduction

3'-deoxy-3'-[<sup>18</sup>F]-fluorothymidine ([<sup>18</sup>F]-FLT), a radiolabeled fluorinated thymidine analog, has been attracting attention as a promising positron emission tomography (PET) tracer for evaluating cell proliferation activity reflecting the ability to synthesize nucleic acid in various malignant tumors [1–4]. [<sup>18</sup>F]-FLT PET has been shown to be useful for preoperative grading and assessing cell proliferation activity in human glioma [4, 5]. In addition, [<sup>18</sup>F]-FLT PET imaging is under investigation to potentially monitor reprogression and response to chemoradiotherapy in postoperative human glioma.

The mechanism of [<sup>18</sup>F]-FLT uptake into cells is based on thymidine metabolism. [<sup>18</sup>F]-FLT can be phosphorylated by thymidine kinase 1 (TK1), a principle enzyme in the salvage pathway of DNA synthesis, and trapped inside proliferative cells [1]. However, [<sup>18</sup>F]-FLT must cross plasma membranes before it can interact with TK1. To interpret [<sup>18</sup>F]-FLT PET images as measures of cell proliferation, we need to understand the mechanisms for its transport, accumulation, and retention in tissues. Efficient cellular uptake requires the presence of specialized plasma membrane nucleoside transporter proteins [6, 7]. The equilibrative nucleoside transporters (ENT) are bidirectional and broadly selective. They catalyze the facilitated diffusion of nucleosides down their concentration gradients

A. Shinomiya (✉) · K. Miyake · M. Okada · T. Nakamura · N. Kawai · T. Tamiya  
Department of Neurological Surgery, Kagawa University  
Faculty of Medicine, 1750-1 Ikenobe, Miki,  
Kagawa 761-0173, Japan  
e-mail: ashinomi@med.kagawa-u.ac.jp

Y. Kushida · R. Haba  
Department of Diagnostic Pathology, Kagawa University  
Faculty of Medicine, Miki, Kagawa, Japan

N. Kudomi  
Department of Physics, Kagawa University  
Faculty of Medicine, Miki, Kagawa, Japan

M. Tokuda  
Department of Cell Physiology, Kagawa University  
Faculty of Medicine, Miki, Kagawa, Japan

[8]. ENT1 is a ubiquitous protein and is the most abundant and widely distributed plasma membrane nucleoside transporter in the human central nervous system [9]. After intravenous injection, FLT distributes rapidly in the extracellular fluid and is transported into the cytosol by nucleoside transporters, probably mainly by the ENT1 [10, 11]. Recent studies report that ENT1 expression might be important for drug toxicity (gemcitabine and capecitabine), and [ $^{18}\text{F}$ ]-FLT uptake also might predict a sensitivity to drug-induced inhibition of nucleic acid synthesis [11–13]. In addition, our recent study demonstrated that [ $^{18}\text{F}$ ]-FLT uptake in the tumor could be significantly related to transport through the disrupted blood–brain barrier (BBB) but not through phosphorylation [14]. Generally, magnetic resonance (MR) imaging after contrast enhancement can be used to evaluate BBB breakdown in the tumor.

On the other hand, angiogenesis is fundamental in tumor growth and progression [15]. A recent study reported a correlation between the imaging of cell proliferation and tumor angiogenesis as reflected by microvessel density (MVD) in lung cancer [16]. Immunohistochemistry for CD34 can be used to determine MVD in malignant tumors.

The aim of our study was to investigate [ $^{18}\text{F}$ ]-FLT uptake and evaluate whether it correlates with ENT1 mRNA expression, microvascular density (CD34 score), or BBB breakdown in human brain glioma.

## Materials and methods

### Patients

Between April 2009 and March 2012, 21 consecutive patients with newly diagnosed gliomas (14 men, 7 women; mean age  $45.2 \pm 17.2$  years, range 21–72 years) were investigated. The use of [ $^{18}\text{F}$ ]-FLT as a PET tracer was approved by Kagawa University Faculty of Medicine, Human Subjects Ethics Committee. Informed consent for [ $^{18}\text{F}$ ]-FLT PET with arterial blood sampling and use of tumor samples for further histological and biochemical analysis was obtained from all patients before the examination. All patients underwent preoperative [ $^{18}\text{F}$ ]-FLT PET kinetic analysis and MR imaging with contrast enhancement usually within 1 week. No patients had had previous treatments except steroid therapy before the PET examination. Histopathology was confirmed in tissue specimens obtained by stereotactic biopsy or resection using a navigation system (StealthStation; Medtronic-Sofamor Danek, Memphis, TN, USA) from the region of interest (ROI) in which [ $^{18}\text{F}$ ]-FLT kinetic parameters were evaluated. All tumors were graded according to the World Health Organization (WHO) grading system (malignancy scale) for central nervous system tumors. Tumor types and grades

were distributed as follows and are listed in Table 1: WHO grade II diffuse astrocytoma ( $n = 3$ ), WHO grade II oligoastrocytoma ( $n = 1$ ), WHO grade III anaplastic astrocytoma ( $n = 5$ ), WHO grade III anaplastic oligodendroglioma ( $n = 1$ ), WHO grade III anaplastic oligoastrocytoma ( $n = 1$ ), and WHO grade IV glioblastoma multiforme ( $n = 10$ ).

### Positron emission tomography scanning procedure

[ $^{18}\text{F}$ ]-FLT was synthesized using an HM-18 cyclotron (Sumitomo Heavy Industries Co., Tokyo, Japan) using a previously reported procedure [12]. The radiochemical purity of the [ $^{18}\text{F}$ ]-FLT produced was  $>95\%$ . The specific activity of [ $^{18}\text{F}$ ]-FLT at the time of patient injection was  $>7.4\text{ GBq}/\mu\text{mol}$  ( $>0.2\text{ Ci}/\mu\text{mol}$ ). Dynamic [ $^{18}\text{F}$ ]-FLT PET scanning was performed using an ECAT EXACT HR + Scanner (Siemens/CTI, Knoxville, TN, USA) in the three-dimensional acquisition mode (collimating septa retracted). The imaging system enables 51 simultaneous transverse acquisitions per field of view (FOV), with intersection spacing of 3 mm, for a total axial FOV of 15 cm. The in-plane reconstructed resolution was 4.7 mm full width at half maximum. [ $^{18}\text{F}$ ]-FLT PET examination was performed 2–14 (mean  $8.5 \pm 3.8$ ) days before surgery. No special dietary instructions were given to patients before examination. Nine patients received steroid treatment for brain edema at the time of PET examination. Images were acquired with patients in the supine position, resting, with their eyes closed. First, a 5-min transmission scan for attenuation correction was obtained using an external source of  $^{68}\text{Ge}$  rod sources rotating around the head. Dynamic emission data were acquired for 60 min ( $4 \times 20\text{ s}$ ,  $4 \times 40\text{ s}$ ,  $4 \times 60\text{ s}$ ,  $4 \times 180\text{ s}$ ,  $8 \times 300\text{ s}$ ) starting immediately after intravenous bolus injection of [ $^{18}\text{F}$ ]-FLT (mean  $279 \pm 72\text{ MBq}$ ). Arterial blood samples were drawn from the brachial artery at 15-s intervals for the first 3 min, followed by increasingly longer intervals to 60 min, to measure arterial plasma radioactivity using an automatic well-type gamma counter (ARC-400, Aloka, Tokyo, Japan). Dynamic PET acquisition data were reconstructed by the filtered back-projection method using a Hanning filter (cutoff frequency, 0.4 cycles per pixel) to generate  $128 \times 128$  matrices.

Static and semiquantitative [ $^{18}\text{F}$ ]-FLT uptake in the tumor was measured by determining the standardized uptake value (SUV). An ROI was set manually by an observer around the hottest area of each lesion or its center located on the MR image if increased [ $^{18}\text{F}$ ]-FLT uptake was absent. The maximum SUV ( $\text{SUV}_{\text{max}}$ ) was regarded as a representative value of [ $^{18}\text{F}$ ]-FLT uptake in each tumor. Alternatively, the tumor to normal brain tissue (T/N) ratio was calculated for evaluating [ $^{18}\text{F}$ ]-FLT uptake in the

**Table 1** Summary of 21 cases with clinical and in vitro data

No.	Age/sex (year)	WHO grade	Dig.	FLT-kinetic			SUV <sub>max</sub>	T/N ratio	MRI + grade (score)	Ki-67 index (%)	CD34 (IHC) (score)	ENT1 (PCR)
				$K_1$ (ml/ min/g)	$k_3$ (/min)	$K_i$ (ml/ min/g)						
1	27/F	4	GBM	0.110	0.090	0.025	1.9	17.27	3	80	2	157
2	26/M	4	GBM	0.039	0.072	0.017	1.88	11.75	3	80	3	570
3	37/M	4	GBM	0.071	0.055	0.012	1.41	8.81	3	20	3	195
4	61/F	4	GBM	0.087	0.151	0.016	1.51	9.44	3	70	2	782
5	28/F	4	GBM	0.090	0.292	0.025	1.53	6.65	2	30	2	112
6	53/M	4	GBM	0.085	0.106	0.027	1.70	9.44	3	25	2	175
7	62/M	4	GBM	0.058	0.093	0.018	1.53	9.00	3	30	2	82
8	67/M	4	GBM	0.061	0.092	0.013	1.45	7.63	3	30	3	279
9	54/M	4	GBM	0.063	0.302	0.024	2.06	9.81	3	40	3	1,414
10	72/M	4	GBM	0.081	0.093	0.019	1.62	9.53	3	50	3	410
1	70/F	3	AA	0.038	0.076	0.007	1.11	6.53	0	30	1	69
2	45/M	3	AA	0.040	0.000	0.000	0.89	6.85	1	10	3	152
3	31/M	3	AA	0.043	0.094	0.015	1.19	10.81	1	20	2	312
4	33/M	3	AA	0.057	0.265	0.020	2.09	13.06	1	70	3	106
5	66/F	3	AA	0.037	0.060	0.006	2.98	10.64	2	15	2	206
6	64/M	3	AO	0.129	0.069	0.013	2.76	19.71	2	50	2	263
7	28/F	3	AOA	0.027	0.047	0.014	0.96	7.38	0	5	1	303
1	31/M	2	DA	0	0	0	0.52	2.36	0	3	2	60
2	36/M	2	OA	0	0	0	0.36	2.57	0	8	1	68
3	37/F	2	DA	0	0	0	0.79	2.72	1	1	2	100
4	21/M	2	DA	0	0	0	0.78	3.12	1	2	2	249

Dig. diagnosis, FLT fluorothymidine, GBM glioblastoma multiforme, AA anaplastic astrocytoma, AO anaplastic oligoastrocytoma, AOA anaplastic oligodendroglioma, OG oligoastrocytoma, DA diffuse astrocytoma, SUV standard uptake value, MRI magnetic resonance imaging, IHC immunohistochemistry, ENT1 equilibrative nucleoside transporter 1, PCR polymerase chain reaction

lesion. The T/N ratio is calculated by dividing the tumor SUV<sub>max</sub> by the mean SUV of contralateral normal gray matter.

#### Kinetic analysis

Kinetic analysis of [<sup>18</sup>F]-FLT PET data was conducted using a two-tissue compartment four-rate parameter model involving blood volume fraction, as previously described [17]. This model is similar to the two-tissue compartmental model for fluorodeoxyglucose (FDG) [18]. The transfer from blood into tissue across the BBB is represented by  $K_1$  (ml/min per gram), whereas the return of [<sup>18</sup>F]-FLT from tissue representing nonphosphorylated [<sup>18</sup>F]-FLT back to the blood is represented by  $k_2$  (/min).  $K_1$  represents transport of [<sup>18</sup>F]-FLT by the nucleoside transporters across the intact BBB in unenhanced tumors, whereas  $K_1$  represents mainly passive [<sup>18</sup>F]-FLT influx through the disrupted BBB in well-enhanced tumors. The metabolic trapping of [<sup>18</sup>F]-FLT through phosphorylation is represented by  $k_3$  (/min) and is the rate-limiting step for its intracellular trapping in tissue. Loss of image signal through these

processes is described by  $k_4$  (/min), which represents dephosphorylation and subsequent efflux via transporters or diffusion. Metabolic flux of [<sup>18</sup>F]-FLT is estimated from parameters derived by fitting the [<sup>18</sup>F]-FLT input function and the total blood activity curve to tissue time-activity curve data. In the calculation, it appears that  $k_4$  is very small compared with  $k_3$ , because the dephosphorylation rate is very low in tumor tissue [17, 18], thus,  $k_4$  was assumed to be zero. Parametric images were calculated using the Lawson–Hanson nonnegative least-squares algorithm. The total metabolic flux constant of [<sup>18</sup>F]-FLT ( $K_i$ ) was estimated from these parameters as:

$$K_i = K_1 \times k_3 / (k_2 + k_3) [\text{ml}/\text{min}/\text{g}].$$

The rate constant values were obtained from the calculated parametric images using ROIs placed, as described above. A parametric image-based method was used for retrieving the [<sup>18</sup>F]-FLT PET kinetic parameters, as the quality of the parametric images was sufficient for evaluation with acceptable noise. This area always contained the maximum [<sup>18</sup>F]-FLT uptake area set for SUV<sub>max</sub> measurement.

## Magnetic resonance imaging

MR images after contrast enhancement were used to evaluate BBB breakdown in the tumor and to identify exact lesion location. T<sub>1</sub>-weighted MR images with 0.1 mmol/kg gadolinium diethylenetriaminepentaacetic acid (Gd-DTPA) were obtained using a 1.5-T whole-body MR imaging unit (Signa Advantage, GE Medical Systems, Milwaukee, WI, USA, or VISART, Toshiba, Tokyo, Japan). The degree of Gd enhancement in the tumor on T<sub>1</sub>-weighted MR images was evaluated visually by comparing the intensity of lesion enhancement with that of the normal choroid plexus [19]. Gd enhancement in tumors was graded as score 0 (none), score 1 (less than that of choroid plexus), score 2 (equal to choroid plexus), and score 3 (more than choroid plexus).

## Real-time polymerase chain reaction (PCR) assay

Total RNA from frozen tumor tissue (5 mm<sup>3</sup> samples) was extracted using Isogen (Nippon Gene, Toyama, Japan), according to the manufacturer's instructions, and quantified by measuring absorbance at 260 nm. Total RNA (1 µg) was reverse-transcribed into complementary DNA (cDNA) using the Prime Script II 1st strand cDNA synthesis Kit (TAKARA Bio Inc, Tokyo, Japan). Quantitative real-time (RT)-PCR was performed using an ABI Prism 7300 RT-PCR system (Applied Biosystems, Carlsbad, CA, USA) with TAKARA Premix Ex Taq Perfect real time (TAKARA Bio Inc, Tokyo, Japan). Primer probes for human ENT1 (hENT1) (*SLC29A1*) and human β-actin as an internal control were purchased from Applied Biosystems (Assay ID: Hs01085706\_m1 and Hs99999903\_m1, respectively). PCR conditions were as follows: initial denaturing at 95 °C for 10 s, followed by 40 cycles of 95 °C for 10 s and 60 °C for 31 s. Reactions were run in triplicate in 96-well plates using standard default settings. Reactive quantification of RNA was determined using the delta–delta Ct method.

## Immunohistochemistry

A representative standard formalin-fixed, paraffin-embedded section (4-µm thick) from each brain tumor specimen was immunohistochemically stained with each primary antibody using the avidin–biotin–peroxidase complex technique and Histofine Simple Stain MAX Peroxidase detection reagent kit designed specifically for immunohistochemical staining on formalin-fixed paraffin-embedded human tissue sections (Nichirei Biochemicals Co, Tokyo, Japan). Primary antibodies were rabbit anti-CD34 (monoclonal; 1:150, Abcam Inc, CA, USA) and mouse anti-Ki-67 (monoclonal; 1:50, Dako, Glostrup, Denmark). Normal rabbit and mouse immunoglobulin G (IgG) was used as negative controls. We performed semiquantitative

immunohistochemistry analysis of CD34 in microvascular endothelial cells on the basis of both the percentage of positive microvessels and the intensity of staining (score 0–3) according to methods described previously [20, 21]. Briefly, in area of the most intense CD34-positive neovascularization, individual microvessel counts (MVCs) were made on a 400× magnification field. Any endothelial cell or endothelial cluster was considered a single countable microvessel. MVC was expressed as an absolute number of microvessels (NMVs) per 400× field for each case. Cases in which NMVs ≤ 5 were considered score 0, 5 < NMV ≤ 15 were score 1, 15 < NMV ≤ 35 were score 2, and NMV > 35 were score 3. This grading procedure was performed by a blinded observer without prior knowledge of data in all cases (Fig. 1).

## Statistical analysis

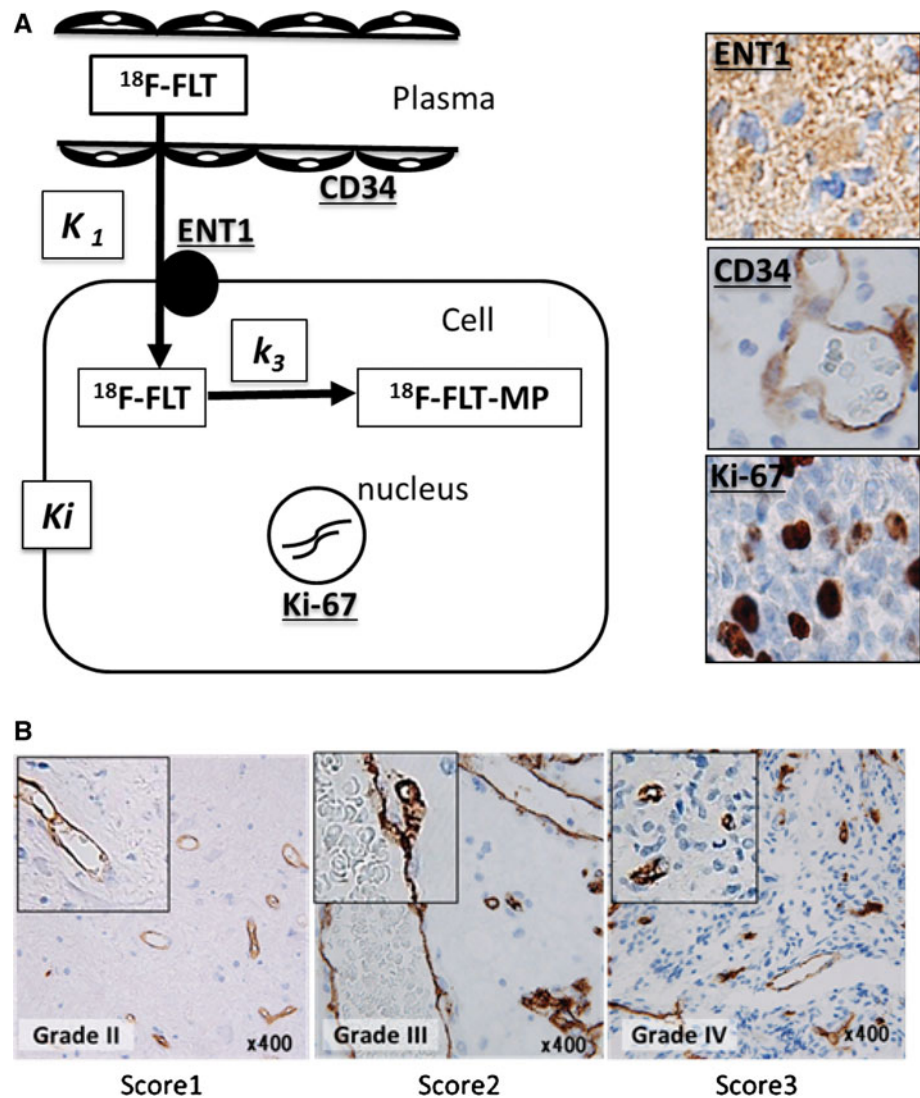
Correlation of the T/N ratio with the Ki-67 index and the [<sup>18</sup>F]-FLT kinetic parameters ( $K_1$ ,  $k_3$ , and  $K_i$ ) were calculated using linear regression analysis. Linear regression analysis was also used to examine whether the [<sup>18</sup>F]-FLT kinetic parameters ( $K_1$ ,  $k_3$ , and  $K_i$ ) were related to ENT1 expression determined by RT-PCR. Correlation of the Gd-enhancement score with  $K_1$ ,  $K_i$ , T/N ratio, Ki-67, ENT1 (RT-PCR), and CD34 score were analyzed using non-parametric Spearman's rank test. The relationship between [<sup>18</sup>F]-FLT kinetic parameters and the grading of immunohistochemical (IHC) staining for CD34 (CD34 score) were also analyzed using the nonparametric Spearman's rank test. All statistical analyses were conducted using statistical analysis software for Excel 2010 (Ekuseru-Toukei 2010; Social Survey Research Information Co., Tokyo). *P* values <0.05 were considered statistically significant.

## Results

Values for kinetic parameters, SUV<sub>max</sub> and T/N ratio, MR imaging and CD34 scores, Ki-67 index and ENT1 mRNA levels are given in Table 1. First, there was a good correlation between the T/N ratio for [<sup>18</sup>F]-FLT and the Ki-67 index, a measure of proliferation ( $r = 0.733$ ,  $p = 0.0002$ ; Fig. 2a). To understand the basis of the increased T/N ratio, we examined the relationship between the composite  $K_i$  with T/N and found good correlation ( $r = 0.61$ ,  $p = 0.0034$ ; Fig. 2b). Changes in  $K_i$  may reflect changes in  $K_1$  (influx across the BBB) and  $k_3$  (phosphorylation of [<sup>18</sup>F]-FLT). There was good correlation between  $K_1$  and T/N ratio ( $r = 0.8042$ ,  $p < 0.0001$ ; Fig. 2c). There was no significant correlation between  $k_3$  and T/N ratio (Fig. 2d).

Next, BBB disruption may cause an increase in  $K_1$  and thus  $K_i$ . Indeed  $K_1$  and  $K_i$  were both significantly correlated with

**Fig. 1 a** A three-compartment model for [ $^{18}\text{F}$ ]-fluorothymidine ([ $^{18}\text{F}$ ]-FLT) kinetics used in this study. Microphotographs shows immunohistochemistry [equilibrative nucleoside transporter 1 (ENT1), CD34, and Ki-67]. **b** Immunohistochemical analysis (score 1–3) of CD34 expression. Gliomatosis showing CD34 expression in microvascular endothelial cells. Number of microvessels (NMVs) per  $\times 400$  field for each case. The cases in which  $\text{NMV} \leq 5$  were considered score 0,  $5 < \text{NMV} \leq 15$  were score 1,  $15 < \text{NMV} \leq 35$  were score 2, and  $\text{NMV} > 35$  were score 3. *Insets* higher magnification



BBB disruption (Gd-enhancement score) ( $p = 0.0004$ , Fig. 3a;  $p = 0.0032$ ; Fig. 3b). In addition, BBB disruption correlated with both T/N ratio and Ki-67 proliferative index ( $p = 0.0111$ , Fig. 3c;  $p = 0.0024$ , Fig. 3d). The Gd-enhancement score also showed significant correlations with ENT1 mRNA levels and CD34 scores ( $p = 0.016$ , Fig. 3e;  $p = 0.007$ , Fig. 3f).

Finally, in contrast to the correlation of  $K_1$  and  $K_i$  with BBB disruption, there was no significant correlation of these two parameters with ENT1 mRNA levels (Fig. 4a, b), although there was a significant relationship between ENT1 and  $k_3$  ( $r = 0.4778$ ,  $p = 0.0285$ , Fig. 4c). There was also no significant correlation of the CD34 score and either  $K_1$ ,  $K_i$  or  $k_3$  (Fig. 5a–c).

## Discussion

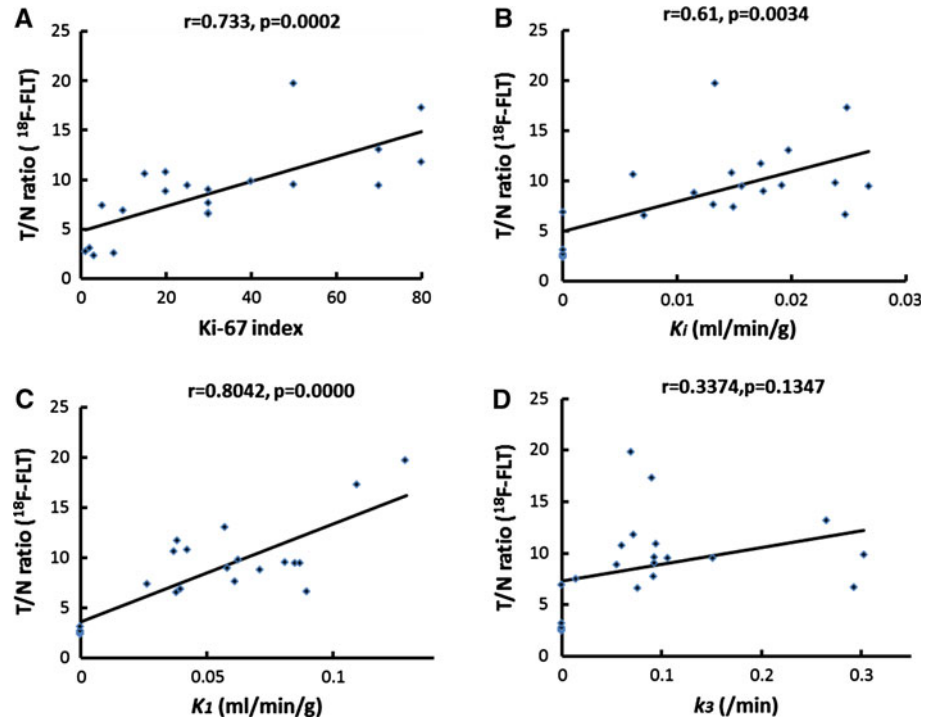
The present study, including 21 patients with glioma, investigated the relationship between [ $^{18}\text{F}$ ]-fluorothymidine

([ $^{18}\text{F}$ ]-FLT) positron emission tomography (PET) kinetic parameters and expression of ENT1 by RT-PCR, microvascular density, and BBB disruption. FLT is an antiretroviral drug that inhibits DNA synthesis [22]. Shields et al. developed [ $^{18}\text{F}$ ]-FLT as a tracer to image proliferation in vivo. They also established [ $^{18}\text{F}$ ]-FLT as an analog substrate of thymidine, which is intracellularly phosphorylated during the S-phase [1].

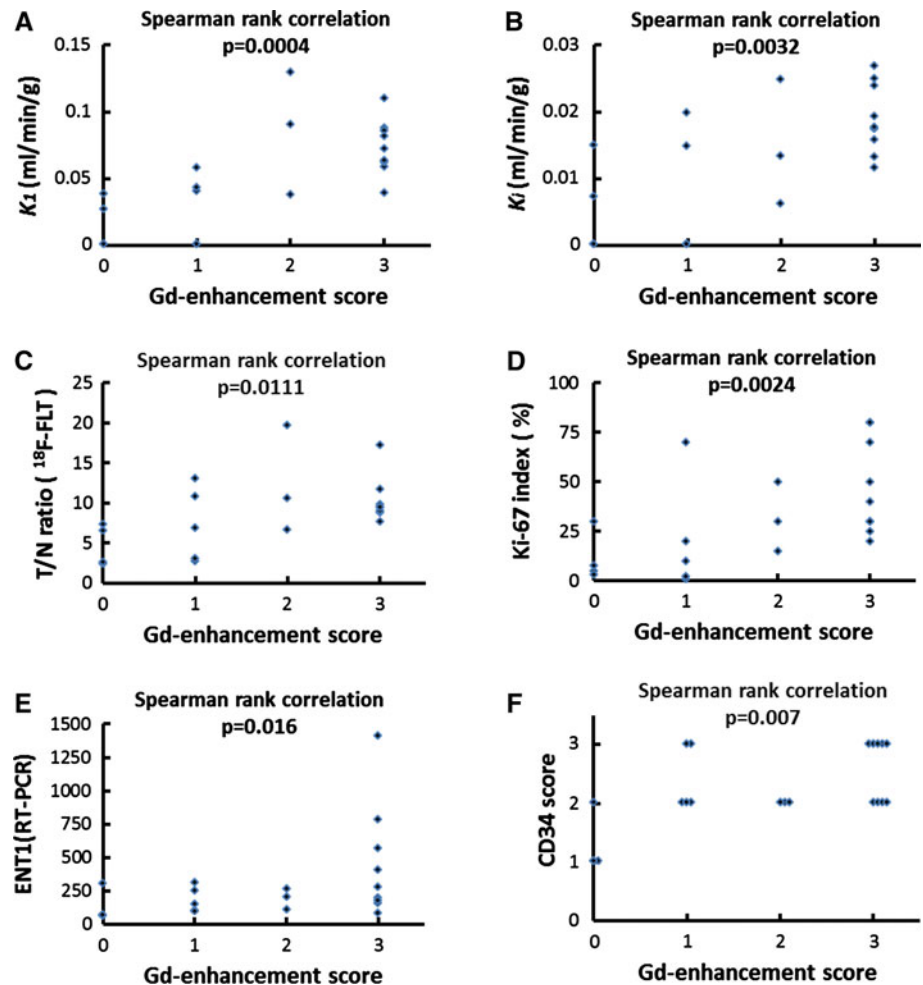
### [ $^{18}\text{F}$ ]-FLT transport in gliomas

This study addressed the hypothesis that the increased [ $^{18}\text{F}$ ]-FLT accumulation in gliomas might reflect changes in ENT1 expression [10, 11]. However, whereas analysis of [ $^{18}\text{F}$ ]-FLT kinetics with PET revealed a correlation between the phosphorylation rate constant  $k_3$  and ENT1 expression, there was no correlation between the influx rate constant  $K_1$  and ENT1 expression. These results suggest that the influx rate constant  $K_1$  might reflect not only [ $^{18}\text{F}$ ]-

**Fig. 2** Linear regression analysis between T/N ratio [ $^{18}\text{F}$ ]-fluorothymidine ( $^{18}\text{F}$ -FLT) and the Ki-67 index, a measure of proliferation, and the [ $^{18}\text{F}$ ]-FLT positron emission tomography (PET) kinetic parameters ( $K_1$ ,  $k_3$  and  $K_i$ ). **a** There was a significant correlation between T/N ratio and Ki-67 index ( $r = 0.733$ ,  $p = 0.0002$ ). **b** There was a correlation between T/N ratio and  $K_i$  ( $r = 0.61$ ,  $p = 0.0034$ ) and **c**  $K_1$  ( $r = 0.8042$ ,  $p < 0.0001$ ), **d** but not  $k_3$



**Fig. 3** Correlation the blood–brain barrier (BBB) breakdown in tumors [gadolinium (Gd) enhancement score] with kinetic parameter ( $K_1$  and  $K_i$ ), T/N ratio, Ki-67, equilibrative nucleoside transporter 1 (ENT1) [real-time polymerase chain reaction (RT-PCR)], and CD34 score using the nonparametric Spearman's rank test. There was a significant correlation of the Gd-enhancement score with **a**  $K_1$  ( $p = 0.0004$ ), **b**  $K_i$  ( $p = 0.0032$ ), **c** T/N ratio ( $p = 0.0111$ ), **d** Ki-67 index ( $p = 0.0024$ ), **e** ENT1 (RT-PCR) ( $p = 0.016$ ), and **f** CD34 score ( $p = 0.007$ )



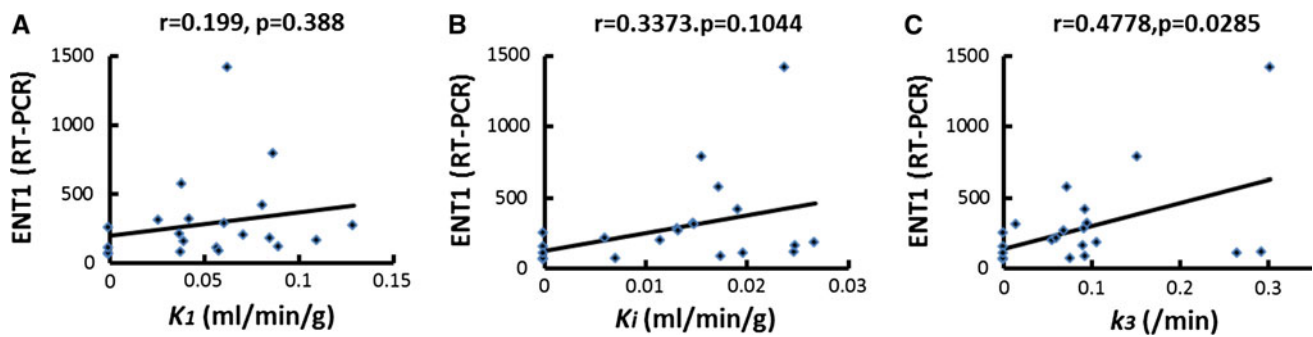


**Fig. 4** Linear regression analysis between equilibrative nucleoside transporter 1 (ENT1) messenger RNA (mRNA) expression by real-time polymerase chain reaction (RT-PCR) and the [ $^{18}\text{F}$ ]-fluorothymidine ([ $^{18}\text{F}$ ]-FLT) positron emission tomography (PET) kinetic parameters ( $K_1$ ,  $K_i$  and  $k_3$ ). There was no correlation between **a**  $K_1$  and **b**  $K_i$ , but **c** there was a correlation between ENT1 (RT-PCR) and  $k_3$  ( $p = 0.0285$ )

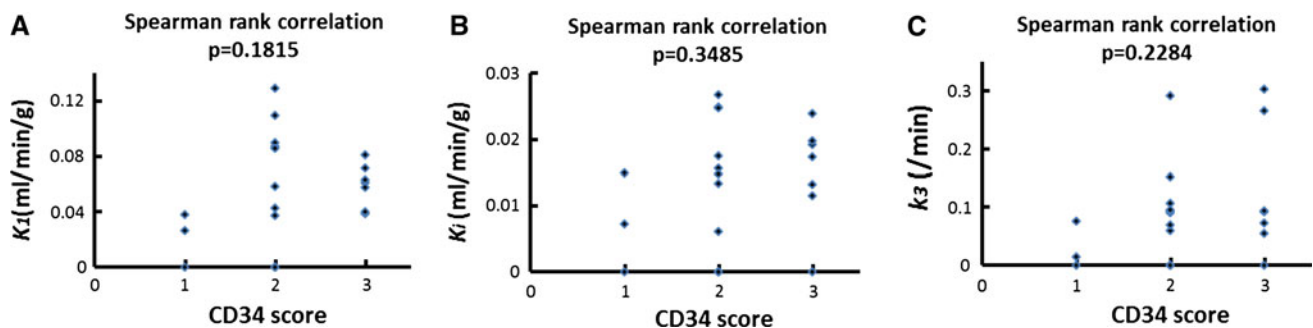


**Fig. 5** Spearman's rank correlation test was used between CD34 score expression by immunohistochemistry and [ $^{18}\text{F}$ ]-FLT PET kinetic parameters ( $K_1$ ,  $K_i$  and  $k_3$ ). There were no correlations between CD34 score and kinetic parameters

FLT accumulation in tumor cells but leakage to extracellular space across the BBB, and the effect of [ $^{18}\text{F}$ ]-FLT uptake via nucleoside transporters on the transport rate constant  $K_1$  might be very small compared with the effect of influx through the disrupted BBB. It might suggest the reason why  $k_3$  relates to ENT1 expression. These results suggest that FLT accumulation might reflect inflammation and postoperative changes.

Ullrich et al. [23] reported that kinetic analysis models with [ $^{18}\text{F}$ ]-FLT PET enable discrimination of increased [ $^{18}\text{F}$ ]-FLT uptake due to increased transport through the BBB. The long half-life of [ $^{18}\text{F}$ ] allows for kinetic analysis, providing differentiation between metabolized and non-metabolized [ $^{18}\text{F}$ ]-FLT in tissue. Kinetic analysis of [ $^{18}\text{F}$ ]-FLT PET imaging was performed to estimate the extent to which [ $^{18}\text{F}$ ]-FLT uptake was due to influx and transport effects across the BBB versus tracer retention related to phosphorylation and tumor growth. Previous studies reported that kinetic analysis of [ $^{18}\text{F}$ ]-FLT PET could clarify whether transport or metabolic trapping largely contributes to the increased accumulation of FLT in tumors [24]. The mathematical aspects of the [ $^{18}\text{F}$ ]-FLT model and the boundary conditions were adopted in our implementation of the previous [ $^{18}\text{F}$ ]-FLT kinetic model [17, 25].

[ $^{18}\text{F}$ ]-FLT and angiogenesis in gliomas

In lung cancer, Yang et al. [16] reported a correlation between [ $^{18}\text{F}$ ]-FLT imaging of cell proliferation and tumor angiogenesis, as reflected by MVD. There are no reports about [ $^{18}\text{F}$ ]-FLT PET and MVD in gliomas. We evaluated whether [ $^{18}\text{F}$ ]-FLT PET kinetics reflected MVD (CD34 score) in gliomas. However, there was no correlation between any of the kinetic parameters and CD34 score. It is possible that CD34 might not be suitable as an MVD marker, as CD34 staining is seen in both mature and immature vessels [16]. Other markers should be examined in the future.

[ $^{18}\text{F}$ ]-FLT and BBB permeability

A previous study showed that the major portion of [ $^{18}\text{F}$ ]-FLT uptake is similar to the low levels observed in unenhanced lesions on MR imaging and demonstrates inside the volume of increased permeability defined by MR imaging  $T_1$ -weighted Gd enhancement [26]. In this study, gliomas with no MR imaging  $T_1$ -weighted Gd enhancement had low accumulation on [ $^{18}\text{F}$ ]-FLT PET images compared with those with enhancement, and there was a good

correlation between [ $^{18}\text{F}$ ]-FLT PET images ( $\text{SUV}_{\text{max}}$ , T/N ratio) and Gd-enhanced MR imaging. In general, Gd contrast enhancement on  $T_1$ -weighted MR images of brain lesions, such as tumor, necrotic tissue, and inflammation, is due to BBB disruption and increased blood vessel permeability [27]. It should be noted that there was some increase in T/N ratio for [ $^{18}\text{F}$ ]-FLT in tumors without Gd enhancement (Table 1), and this remains to be understood. [ $^{18}\text{F}$ ]-FLT can cross the BBB and plasma membranes; however, the mechanisms of transport and influx to tumor cells across the BBB in vivo have not been fully elucidated. To interpret [ $^{18}\text{F}$ ]-FLT PET images as a measure of cell proliferation, we need to understand the mechanisms that account for its transport, accumulation, and retention in tissues.

## Conclusions

This study demonstrates that [ $^{18}\text{F}$ ]-FLT uptake in newly diagnosed human brain gliomas is related to transport through the disrupted BBB but not to phosphorylation activity. Although tissue ENT1 expression reflects the phosphorylation rate constant  $k_3$ , the transport rate constant  $K_1$  determined by [ $^{18}\text{F}$ ]-FLT PET kinetic analysis did not accurately reflect ENT1 expression and should not be used as a surrogate biomarker of transport activity in human brain gliomas. Several MVD markers should be examined in future studies.

**Acknowledgments** This study was supported by a Grant-in-Aid for Scientific Research from the Japanese Society for the Promotion of Science. We thank Prof. Richard F. Keep (Department of Neurosurgery and Physiology, University of Michigan) for providing useful suggestions.

**Conflict of interest** None.

## References

- Shields AF, Grierson JR, Dohmen BM et al (1998) Imaging proliferation in vivo with [ $^{18}\text{F}$ ]-FLT and positron emission tomography. *Nat Med* 4:1334–1336
- Buck AK, Schirmeister H, Hetzel M et al (2002) 3-deoxy-3-[( $^{18}\text{F}$ )] fluorothymidine-positron emission tomography for non-invasive assessment of proliferation in pulmonary nodules. *Cancer Res* 62:3331–3334
- Wagner M, Seitz U, Buck A et al (2003) 3'-[ $^{18}\text{F}$ ]fluoro-3'-deoxythymidine([ $^{18}\text{F}$ ]-FLT) as positron emission tomography tracer for imaging proliferation in murine B-Cell lymphoma model and in the human disease. *Cancer Res* 63:2681–2687
- Chen W, Cloughesy T, Kamdar N et al (2005) Imaging proliferation in brain tumors with [ $^{18}\text{F}$ ]-FLT PET: comparison with [ $^{18}\text{F}$ ]-FDG. *J Nucl Med* 46:945–952
- Miyake K, Shinomiya A, Okada M et al (2012) Usefulness of FDG, MET and FLT-PET studies for the management of human gliomas. *J Biomed Biotechnol* 2012:205818. doi:10.1155/2012/205818
- Baldwin SA, Mackey JR, Cass CE, Young JD (1999) Nucleoside transporters: molecular biology and implications for therapeutic development. *Mol Med Today* 5:216–224
- Mackey JR, Yao SYM, Smith KM et al (1999) Gemcitabine transport in *Xenopus* oocytes expressing recombinant plasma membrane mammalian nucleoside transporters. *J Natl Cancer Inst* (Bethesda) 91:1876–1881
- Pastor-Anglada M, Cano-Soldado P, Molina-Arcas M et al (2005) Cell entry and export of nucleoside analogues. *Virus Res* 107:151–164
- Jennings LL, Hao C, Cabrita MA et al (2001) Distinct regional distribution of human equilibrative nucleoside transporter proteins 1 and 2 (hENT1 and hENT2) in the central nervous system. *Neuropharmacology* 40:722–731
- Paproski RJ, Ng AML, Yao SYM et al (2008) The role of human nucleoside transporters in uptake of 3'-deoxy-3'-fluorothymidine. *Mol Pharmacol* 74:1372–1380
- Paproski RJ, Young JD, Cass CE (2010) Predicting gemcitabine transport and toxicity in human pancreatic cancer cell lines with the positron emission tomography tracer 3'-deoxy-3'-fluorothymidine. *Biochem Pharmacol* 79:587–595
- Mackey JR, Jennings LL, Clarke ML et al (2002) Immunohistochemical variation of human equilibrative nucleoside transporter 1 protein in primary breast cancers. *Clin Cancer Res* 8:110–116
- Santini D, Perrone G, Vincenzi B et al (2008) Human equilibrative nucleoside transporter 1 (hENT1) protein is associated with short survival in resected ampullary cancer. *Ann Oncol* 19:724–728
- Shinomiya A, Kawai N, Okada M et al (2013) Evaluation of 3'-deoxy-3'-[ $^{18}\text{F}$ ]-fluorothymidine ( $^{18}\text{F}$ -FLT) kinetics correlated with thymidine kinase-1 expression and cell proliferation in newly diagnosed gliomas. *Eur J Nucl Med Mol Imaging* 40:175–185
- Hanahan D, Folkman J (1996) Patterns and emerging mechanisms of the angiogenic switch during tumorigenesis. *Cell* 86:353–364
- Yang W, Zhang Y, Zheng Fu et al (2012) Imaging proliferation of 18F-FLT PET/CT correlated with the expression of microvessel density of tumor tissue in non-small-cell cancer. *Eur J Nucl Med Mol Imaging* 39:1289–1296
- Muzi M, Spence AM, O'Sullivan F et al (2006) Kinetic analysis of 3'-deoxy-3'-18F-fluorothymidine in patients with gliomas. *J Nucl Med* 47:1612–1621
- Kudomi N, Järvisalo MJ, Kiss J et al (2009) Non-invasive estimation of hepatic glucose uptake from [ $^{18}\text{F}$ ]FDG PET images using tissue-derived input functions. *Eur J Nucl Med Mol Imaging* 36:2014–2026
- Hong IK, Kim JH, Ra YS et al (2011) Diagnostic usefulness of 3'-deoxy-3'-[ $^{18}\text{F}$ ]fluorothymidine positron emission tomography in recurrent brain tumor. *J Comput Assist Tomogr* 35:679–684
- Zhen HN, Zhang x, Hu PZ et al (2005) Survival expression and its relation with proliferation, apoptosis, and angiogenesis in brain gliomas. *Cancer* 104:2775–2783
- Okubo S, Zhen HN, Kawai N (2010) Correlation of L-methyl-11C-methionine (MET) uptake with L-type amino acid transporter 1 in human gliomas. *J Neurooncol* 99:217–225
- Flexner C, van der Horst C, Jacobson MA et al (1994) Relationship between plasma concentrations of 3'-deoxy-3'-fluorothymidine (alovudine) and antiretroviral activity in two concentration-controlled trials. *J Infect Dis* 170:1394–1403
- Ullrich R, Backers H, Li H et al (2008) Glioma proliferation as assessed by 3'-fluoro-3'-deoxy- L-thymidine positron emission tomography in patients with newly diagnosed high-grade glioma. *Clin Cancer Res* 14:2049–2055
- Jacobs AH, Thomas A, Kracht LW et al (2005) 18F-fluoro-L-thymidine and 11C-methylmethionine as markers of increased



- transport and proliferation in brain tumors. *J Nucl Med* 46: 1948–1958
25. Visvikis D, Francis D, Mulligan R et al (2004) Comparison of methodologies for the in vivo assessment of <sup>18</sup>FFLT utilisation in colorectal cancer. *Eur J Nucl Med Mol Imaging* 31:169–178
26. Davis WK, Boyko OB, Hoffman JM et al (1993) [<sup>18</sup>F]2-fluoro-2-deoxyglucose-positron emission tomography correlation of gadolinium-enhanced MR imaging of central nervous system neoplasia. *ANJR Am J Neuroradiol* 14:515–523
27. Hesselink JR, Press GA (1988) MR contrast enhancement of intracranial lesions with Gd-DTPA. *Radiol Clin North Am* 26:873–887